Ultracold molecular collisions in combined electric and magnetic fields

Goulven Quéméner*
Laboratoire Aimé Cotton, CNRS, Université Paris-Sud, ENS Cachan, Campus d'Orsay, Bâtiment 505, 91405 Orsay, France

John L. Bohn
JILA, NIST, and Department of Physics, University of Colorado, Boulder, Colorado 80309, USA
(Received 20 June 2013; published 15 July 2013)

We consider collisions of electric and magnetic polar molecules, taking the OH radical as an example, subject to combined electric and magnetic static fields. We show that the relative orientation of the fields has an important effect on the collision processes for different fields' magnitudes at different collision energies. This is due to the way the molecules polarize in the combined electric and magnetic fields and hence the way the electric dipole-dipole interaction rises. If OH molecules are confined in magnetic quadrupole traps and if an electric field is applied, molecular collisions will strongly depend on the position as well as the velocity of the molecules. Consequences on the molecular dynamics are discussed.

DOI: 10.1103/PhysRevA.88.012706 PACS number(s): 34.50.Cx

I. INTRODUCTION

Cold molecules, with translational temperatures at or below 100 mK, are strongly subject to control over their behavior and may afford unprecedented opportunities for probing chemistry as a function of initial conditions to reaction [1]. Thus, for example, μK samples of KRb molecules have been formed [2] and their reactions probed for different temperatures [3], electric fields [4], and dimensional confinements [5,6]. These molecules have appreciable electric dipole moments, so manipulation of their collisions arises from their comparatively strong dipolar interactions.

More broadly, open-shell radicals can also be produced at low temperatures, albeit in samples not quite as cold. Examples include $^2\Sigma$ molecules such as SrF [7] or $^2\Pi$ molecules such as OH [8]. In addition to being of arguably greater chemical interest, these species present the possibility of simultaneous control by acting on their magnetic, as well as electric, dipole moments. The simultaneous action of electric and magnetic fields has been considered previously in the context of buffer-gas-cooled species, considering collisions such as He + CaD and He + ND [9–11] or He + YbF [12]. For certain radicals, such as OH, O_2, and NH, molecule-molecule collisions have been considered in the presence of either electric [13] or magnetic [14–19] fields but not both simultaneously.

Here we consider the effect of both electric and magnetic fields on collisions of the OH radical, at collision energies ranging from 1 μK to 50 mK. In its ground electronic state, this molecule possesses a magnetic dipole moment of $|\vec{\mu}| = 2\mu_B$ (μ_B is the Bohr magneton) and an electric dipole moment of $|\vec{d}| = 1.67$ D (D is the Debye unit). Thus, at the temperatures considered, long-range electric dipole forces generate interaction energies that can exceed translational temperatures when the molecules are hundreds of Bohr radii apart. This circumstance implies that electric and magnetic fields act on the molecules primarily on this distance scale and that theoretical models focusing on this long-range physics are adequate to see the effect of the fields. From this standpoint, it has already been noted that electric fields tend to *increase* the rate of state-changing collisions of OH molecules [13], while magnetic fields tend to *decrease* these rates [14]. If both types of field are present, they are therefore in competition, promising additional opportunities for manipulation of collisions. In particular, the angle between the fields, at the site of a collision, can be decisive in determining the collision's outcome.

The emphasis on long-range physics is assisted by the special characteristics of $^2\Pi$ molecules such as OH. For Σ molecules, the electric dipole moment is induced by the mixing of the ground and the excited rotational states by an electric field. The rotational constant is on the order of mK so the ground and higher excited rotational levels cannot be treated independently, while for OH molecules the large rotation splitting implies small mixing of higher-lying rotational states at modest electric fields. A signature of this feature is the protection of certain low-field-seeking states of cold OH molecules in a magnetic field, leading to high elastic collisions compared to inelastic collisions, stemming from a strong repulsive van der Waals coefficient [8]. Because of this repulsion, the OH molecules in those states are expected to be shielded from chemical reactions at sufficiently low temperature.

In this paper, we investigate the scattering of polar molecules when arbitrarily combined electric and magnetic fields are applied (parallel as well as nonparallel fields), taking the OH molecule as an example. This study is the starting point to more complicated dynamics of polar molecules in a quadrupole magnetic trap in the presence of an electric field as performed in ongoing experiments [20], where collisions of molecules will occur at different electric and magnetic field configurations for different positions in the trap. These collisions are also important to determine new efficient evaporative cooling schemes, for example, using appropriate electric and magnetic field trap combinations, to further cool down molecular dipolar gases. If quantum degenerate gases are finally produced, the combined electric and magnetic fields can be used as additional tools to control and probe the many-body physics of electric and magnetic dipolar systems [21–23].

The paper is organized as follows. In Sec. II, we describe the time-independent quantum formalism used to perform the

*goulven.quemener@u-psud.fr

scattering calculations, presented in Sec. III. We summarize in Sec. IV.

II. SCATTERING IN COMBINED ELECTRIC AND MAGNETIC FIELDS

We present here the time-independent quantum formalism used in this work for the scattering of two OH molecules in arbitrary combined electric fields.

A. Molecular energies and functions

The OH molecule in its ground rovibronic state $^2\Pi_{3/2},v=0,j=3/2$ is well described by a Hund case (a) scheme. Here j is the quantum number associated with its rotational angular momentum $\vec{j}$, m_j is its projection onto the laboratory space-fixed axis with unit vector $\hat{Z}$, and ω_j is its projection onto the molecular body-fixed axis with unit vector $\hat{z}$. In its ground state, $\omega_j=\pm 3/2$ is the sum of $\lambda=\pm 1$ and $\sigma=\pm 1/2$, the values of the projection of the electronic orbital $\vec{l}$ and spin $\vec{s}$ angular momentum onto the body-fixed axis. A good basis set for Hund's case (a) molecule is therefore $|j,m_j,\omega_j\rangle|\lambda,\sigma\rangle$ [24]. The molecule exhibits a small Λ doublet of $\Delta\approx 80$ mK between two states e and f of different parity within its ground rovibronic state $^2\Pi_{3/2},v=0,j=3/2$. The electric field mixes these two states to induce the electric dipole moment in the laboratory frame. The next rotational level $^2\Pi_{3/2},v=0,j=5/2$ is $\simeq$100 K higher than the $j=3/2$ state, so the OH ground rotational state is well separated from all its higher excited states and will be ignored in the rest of the study considering the low-collision-energy range of the molecules.

In Hund's case (a), the magnetic dipole moment is given to a good approximation by $\vec{\mu}=-\mu_B(g_s\sigma+g_l\lambda)\hat{z}$, where μ_B is the Bohr magneton, g_s is the electron's g factor ($g_s\sim 2.002\approx 2$) and $g_l=1$, so that $\vec{\mu}\approx\pm 2\mu_B\hat{z}$. The electric dipole moment is given by $\vec{d}=d\hat{z}$, with $d=1.67$ D. As a consequence, in a Hund case (a) scheme, both electric and magnetic dipole moments lie along the molecular axis, as depicted schematically in Fig. 1 (if the dipoles point in the same direction). This implies that we do not take into account couplings between the states $|\omega_j|=3/2$ and $1/2$. This is not important in this study since the first $|\omega_j|=1/2$ state lies well above the ground state by more than 100 K [24].

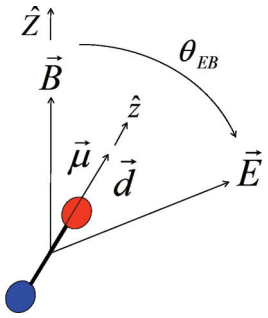

FIG. 1. (Color online) Schematic electric and magnetic dipole moments for an OH molecule in a Hund case (a) scheme, in the presence of an arbitrary electric and magnetic field configuration $\vec{E},\vec{B},\theta_{EB}$.

When a magnetic field is applied, the interaction of the molecule with the field is given by the Zeeman Hamiltonian $H_Z=-\vec{\mu}\cdot\vec{B}$. In the Hund case (a) basis set $|j,m_j,\omega_j\rangle$ (we ignore the spectator ket $|\lambda,\sigma\rangle$ in the following unless stated otherwise and we take $\omega_j=\omega_j'$), it takes the form

$$\begin{aligned}&\langle j,m_j,\omega_j|H_Z|j',m_j',\omega_j\rangle\\&=-\mu B(-1)^{m_j-\omega_j}\sqrt{2j+1}\sqrt{2j'+1}\\&\times\begin{pmatrix}j&1&j'\\-\omega_j&0&\omega_j\end{pmatrix}\begin{pmatrix}j&1&j'\\-m_j&0&m_j'\end{pmatrix},\end{aligned}\quad(1)$$

with $\mu=-\mu_B(g_s\sigma+g_l\lambda)$. Here we choose $\vec{B}$ to point along the space-fixed frame axis $\hat{Z}$ (as shown in Fig. 1). Based on the symmetry of the three-j symbols, we must have $j'-j=\Delta j=0,\pm 1$ and $m_j'=m_j$.

When an electric field is applied, the interaction of the molecule with the field is given by the Stark Hamiltonian $H_S=-\vec{d}\cdot\vec{E}$ and in the Hund case (a) basis set, it takes the form

$$\begin{aligned}&\langle j,m_j,\omega_j|H_S|j',m_j',\omega_j\rangle\\&=-dE\sqrt{\frac{4\pi}{3}}Y_{1,m_j'-m_j}(\theta_{EB},\phi_{EB})(-1)^{m_j-\omega_j}\sqrt{2j+1}\\&\times\sqrt{2j'+1}\begin{pmatrix}j&1&j'\\-\omega_j&0&\omega_j\end{pmatrix}\begin{pmatrix}j&1&j'\\-m_j&m_j-m_j'&m_j'\end{pmatrix}\end{aligned}\quad(2)$$

if we allow $\vec{E}$ to point in an arbitrary direction (θ_{EB},ϕ_{EB}) from the $\hat{Z}$ axis (as shown in Fig. 1). In the following we will set $\phi_{EB}=0$. From the three-j symbols, we must have again $j'-j=\Delta j=0,\pm 1$, but now, if there is a nonzero angle θ_{EB} between the $\vec{E}$ field and the $\vec{B}$ field, we have in general $m_j'-m_j=0,\pm 1$. Thus the quantum numbers m_j referring to a particular axis (the $\vec{B}$ or the $\vec{E}$ axis) are no longer good. Good quantum numbers can be found along two particular axes as shown in Ref. [25], but we do not do so here. Note that if $\theta_{EB}=\pi/2$, $m_j'=m_j\pm 1$ and if $\theta_{EB}=0$, we recover the case $m_j'=m_j$.

In the absence of rotation, molecules with the quantum numbers $\lambda=\pm 1$ have the same energy causing a Λ-doubling degeneracy for $\lambda\geqslant 1$. An additional term H_Λ stemming from the coupling of the rotation and the electronic angular momentum of the molecule splits this Λ doubling into two distinct states e and f of different parity [24]. A good basis set is then the parity basis set

$$\begin{aligned}&|j,m_j,|\omega_j|,\epsilon\rangle||\lambda|,|\sigma|\rangle\\&=\frac{1}{\sqrt{2}}\{|j,m_j,\omega_j\rangle|\lambda,\sigma\rangle+\epsilon|j,m_j,-\omega_j\rangle|-\lambda,-\sigma\rangle\},\end{aligned}\quad(3)$$

with $\epsilon=\pm 1$ corresponding, respectively to the e or f states parities [26]. For OH, the f-e splitting is about $\Delta\approx 80$ mK

and is diagonal in the parity basis,

$$\langle j,m_j,|\omega_j|,\epsilon|H_\Lambda|j',m_j',|\omega_j|,\epsilon'\rangle = (-\epsilon)\Delta/2\,\delta_{j,j'}\delta_{m_j,m_j'}\delta_{\epsilon,\epsilon'}. \tag{4}$$

The Zeeman expression (1) in this new basis set is given by

$$\begin{aligned}&\langle j,m_j,|\omega_j|,\epsilon|H_Z|j',m_j',|\omega_j|,\epsilon'\rangle \\ &= -\mu B\,\delta_{\epsilon,\epsilon'}(-1)^{m_j-|\omega_j|}\sqrt{2j+1}\sqrt{2j'+1} \\ &\quad\times\begin{pmatrix} j & 1 & j' \\ -|\omega_j| & 0 & |\omega_j|\end{pmatrix}\begin{pmatrix} j & 1 & j' \\ -m_j & 0 & m_j'\end{pmatrix},\end{aligned} \tag{5}$$

with $\mu = -\mu_B(g_s|\sigma| + g_l|\lambda|) \approx -2\mu_B$. The magnetic field mixes states of the same parity $\epsilon = \epsilon'$ only. The Stark expression (2) is given by

$$\begin{aligned}&\langle j,m_j,|\omega_j|,\epsilon|H_S|j',m_j',|\omega_j|,\epsilon'\rangle \\ &= -dE(1-\delta_{\epsilon,\epsilon'})\sqrt{\frac{4\pi}{3}}Y_{1,m_j'-m_j}(\theta_{EB},\phi_{EB})(-1)^{m_j-\omega_j} \\ &\quad\times\sqrt{2j+1}\sqrt{2j'+1}\begin{pmatrix} j & 1 & j' \\ -|\omega_j| & 0 & |\omega_j|\end{pmatrix} \\ &\quad\times\begin{pmatrix} j & 1 & j' \\ -m_j & m_j-m_j' & m_j'\end{pmatrix}.\end{aligned} \tag{6}$$

The electric field mixes states of the different parity $\epsilon \neq \epsilon'$ only. The selection rules $\Delta j = 0, \pm 1$ and $\Delta m_j = 0, \pm 1$ still hold. In the following, we take $j = j' = 3/2$.

The diagonalization of the molecular Hamiltonian $H_\Lambda + H_Z + H_S$ in the parity basis set given by expressions (4)–(6) leads to the eight eigenenergies denoted ε_i, with $i = 1, \ldots, 8$ from lowest to highest energy, and eigenfunctions denoted $|i\rangle$ of the OH molecule in a combined electric and magnetic field with a relative orientation θ_{EB}. These energies are shown in Fig. 2 for a fixed magnetic field of $B = 500$ G as a function of the electric field E for the three angles $\theta_{EB} = 0$ (black curves, parallel fields), $\theta_{EB} = \pi/4$ [green (light gray) curves, neither parallel nor perpendicular], and $\theta_{EB} = \pi/2$ [red (dark gray) curves, perpendicular fields].

For the highest excited adiabatic state $|8\rangle$ represented by the highest-energy curve, it is easier to induce an electric dipole moment when the electric field is more parallel to the magnetic field axis, while it is harder when the fields are more perpendicular. This can be seen from the derivative of the energy curves with respect to the electric field that is proportional to the induced electric dipole moment. The derivative for the $\theta_{EB} = \pi/2$ red (dark gray) curve is smaller than that for the $\theta_{EB} = 0$ black curve, with the one for the $\theta_{EB} = \pi/4$ green (light gray) curve sitting in between. In terms of the results of Ref. [25], the induced electric dipole moment $\tilde{d}$ for the upper adiabatic state $|8\rangle$ can be approximated by

$$\tilde{d} \approx \frac{|\omega_j m_j|}{j(j+1)}\left(1 + \frac{\mu B}{dE}\cos(\theta_{EB})\right)d. \tag{7}$$

Then, if θ_{EB} goes from 0 to $\pi/2$, $\tilde{d}$ decreases in magnitude for fixed B and E fields, as seen in Fig. 2.

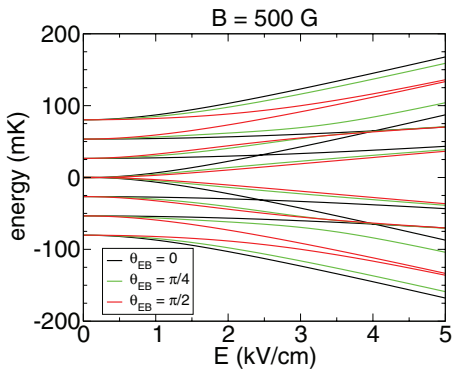

FIG. 2. (Color online) Eigenenergies of the ground-state OH molecule in combined electric and magnetic fields as a function of the electric field for $\theta_{EB} = 0$ (black curve), $\theta_{EB} = \pi/4$ [green (light gray) curve], and $\theta_{EB} = \pi/2$ [red (dark gray) curve]. The magnetic field is $B = 500$ G.

B. Molecular scattering

In what follows we will be concerned with molecules colliding in their stretched states $|8\rangle$, which are magnetically trapped. In collisions, these molecules will exert torques on one another that can disturb their orientation, producing molecules in states $|i < 8\rangle$ and in general leading to trap loss and heating. As these appear to be the dominant loss collisions [8], we focus on them and ignore the possibility of chemical reactions. Our scattering theory is therefore similar to the long-range-dominated theories in Refs. [15,27].

We consider two OH molecules of mass m_1, m_2 and position $\vec{r}_1, \vec{r}_2$, respectively. We decouple the motion of the two-body system into a motion of a center of mass, of total mass $m_{\rm tot} = m_1 + m_2$ and position $\vec{R} = (m_1\vec{r}_1 + m_2\vec{r}_2)/(m_1 + m_2)$, and a motion of a relative particle, of reduced mass $m_{\rm red} = (m_1 m_2)/(m_1 + m_2)$ and position $\vec{r} = \vec{r}_2 - \vec{r}_1$. The total Hamiltonian of the relative motion is $H = T + V$, with T being the relative kinetic energy operator of the relative motion and V the potential energy. The long-range electric dipole-dipole interaction is given by

$$V = \frac{\vec{d}_1\cdot\vec{d}_2 - 3(\vec{d}_1\cdot\hat{r})(\vec{d}_2\cdot\hat{r})}{4\pi\varepsilon_0 r^3}. \tag{8}$$

We do not consider the magnetic dipole-dipole interaction since it is of the order of $\alpha^2 \approx 10^{-4}$ smaller than the electric dipole-dipole interaction. Because the molecules are identical (same isotope and same mass), we construct an overall wave function Ψ of the system for which the molecular permutation operator P gives $P\Psi = \epsilon_P\Psi$, with $\epsilon_P = +1$ for bosonic molecules and $\epsilon_P = -1$ for fermionic molecules. In this study, we consider ^{16}OH bosonic molecules so that $\epsilon_P = +1$. This is due to a total spin $\vec{f} = \vec{j} + \vec{i}$ with integer quantum numbers $f = 1,2$, where $\vec{i}$ is the nuclear spin of the molecule ($i = 1/2$) and $\vec{j}$ the total angular momentum ($j = 3/2$) of the molecule considered. We assume that the nuclear spin i and the angular momentum j are decoupled. This is a good approximation for strong magnetic fields $\mu B \gg \Delta_{\rm hf}$ or high collision energies $E_c \gg \Delta_{\rm hf}$, where $\Delta_{\rm hf} \approx 4$ mK is the hyperfine energy splitting between the $f = 1$ and 2 manifolds. For the state we consider, this assumption is valid for most of the results presented here especially when $B \gg 100$ G. Note that the hyperfine

structure was previously considered in OH cold collisions that focused on smaller collision energies and smaller magnetic fields [13,14].

We construct symmetrized states of the internal wave function of the combined molecular states $|i_1\rangle|i_2\rangle$ of two OH molecules with energies $\varepsilon_{i_1}+\varepsilon_{i_2}$ ($i_1,i_2=1,\ldots,8$),

$$|i_1,i_2,\eta\rangle = \frac{1}{\sqrt{2(1+\delta_{i_1,i_2})}}[|i_1,i_2\rangle + \eta|i_2 i_1\rangle] \tag{9}$$

for which $P|i_1,i_2,\eta\rangle = \eta|i_1,i_2,\eta\rangle$. Here η is a good quantum number and is conserved during the collision. If the molecules are in the same molecular internal state, only the symmetry $\eta=+1$ has to be considered. If they are in different internal state, both symmetries $\eta=\pm 1$ have to be considered. As we consider both initial OH molecules in their highest eigenstate $|8\rangle$ in the combined electric and magnetic field, the molecules are indistinguishable and $\eta=+1$. The total wave function $\Psi(\vec{r})$ with $\vec{r}=\{r,\theta,\varphi\}$ is expanded onto a basis set of spherical harmonics $Y_{l,m_l}(\theta,\varphi)$ corresponding to the orbital angular momentum of the colliding particles

$$\begin{aligned}\Psi_k(r,\theta,\varphi) &= \sum_{k''=1}^{N_{\rm tot}} \frac{1}{r} F_{k''k}(r) Y_{l'',m_l''}(\theta,\varphi)|i_1'' i_2'',\eta''\rangle \\ &= \sum_{k''=1}^{N_{\rm tot}} \frac{1}{r} F_{k''k}(r)|i_1'' i_2'',l'',m_l'',\eta''\rangle,\end{aligned} \tag{10}$$

where $k=i_1,i_2,l,m_l,\eta$ and $N_{\rm tot}$ is the total number of diabatic channels we use in our calculation.

Symmetry considerations can restrict the number of channels required. Because $\eta=+1$, and to satisfy $P\Psi=\epsilon_P\Psi$ with $\epsilon_P=+1$, l must take even values. In this study we consider only the partial waves $l=0,2,4,6,8$, finding these sufficient to converge the results at the collision energies investigated here. The total number of channels is typically $N_{\rm tot}=1620$. Moreover, when the fields are parallel, the total quantum number $M=m_{j_1}+m_{j_2}+m_l$ is conserved and $N_{\rm tot}=118$ for the $M=+3$ components for the initial states $m_{j_1}=3/2$, $m_{j_2}=3/2$, $m_l=0$ for example. The total energy E is equal to the sum $\varepsilon_{i_1}+\varepsilon_{i_2}+E_c$, where E_c is the initial collision energy. The total energy E is conserved during the collision. We choose the zero of energy to be equal to $\varepsilon_8+\varepsilon_8$, the energy of our initial molecular states. The time-independent Schrödinger equation $H\Psi=E\Psi$ provides a diabatic set of close-coupling differential equations for the radial functions $F_{k'k}(r)$ from a state k to a state k',

$$\begin{aligned}&\left\{-\frac{\hbar^2}{2m_{\rm red}}\frac{d^2}{dr^2}+\frac{\hbar^2 l(l+1)}{2m_{\rm red}r^2}-E\right\}F_{k'k}(r) \\ &\quad+\sum_{k''=1}^{N_{\rm tot}}\mathcal{U}_{k'k''}(r)\,F_{k''k}(r)=0,\end{aligned} \tag{11}$$

where

$$\mathcal{U}_{k'k''}(r)=\langle i_1',i_2',l',m_l',\eta'|V_{\rm dd}|i_1'',i_2'',l'',m_l'',\eta''\rangle. \tag{12}$$

Using Eq. (9) and the fact that the individual molecular eigenstates $|i_1\rangle$ and $|i_2\rangle$ in Eq. (3) are linear combinations of the basis sets $|j_1,m_{j_1},|\omega_{j_1}|,\epsilon\rangle$ and $|j_2,m_{j_2},|\omega_{j_2}|,\epsilon\rangle$ after diagonalization, we can obtain the coupling matrix elements $\mathcal{U}_{k'k''}(r)$ knowing that the dipole-dipole interaction in the Hund case (a) molecule-molecule basis set $|j_1,m_{j_1},\omega_{j_1},j_2,m_{j_2},\omega_{j_2},l,m_l\rangle$ is expressed by

$$\begin{aligned}&\langle j_1,m_{j_1},\omega_{j_1},j_2,m_{j_2},\omega_{j_2},l,m_l|V_{\rm dd}|j_1',m_{j_1}',\omega_{j_1},j_2',m_{j_2}',\omega_{j_2},l',m_l'\rangle \\ &=-\frac{\sqrt{30}d_1d_2}{4\pi\varepsilon_0 r^3}(-1)^{m_{j_1}-\omega_{j_1}}(-1)^{m_{j_2}-\omega_{j_2}}(-1)^{m_l}\sqrt{2j_1+1}\sqrt{2j_2+1}\sqrt{2l+1}\sqrt{2j_1'+1}\sqrt{2j_2'+1}\sqrt{2l'+1} \\ &\times\sum_{p=-2}^{2}\sum_{p_1=-1}^{1}\sum_{p_2=-1}^{1}\begin{pmatrix}1&1&2\\p_1&p_2&-p\end{pmatrix}\begin{pmatrix}l&2&l'\\0&0&0\end{pmatrix}\begin{pmatrix}l&2&l'\\-m_l&m_l-m_l'&m_l'\end{pmatrix}\begin{pmatrix}j_1&1&j_1'\\-\omega_{j_1}&0&\omega_{j_1}\end{pmatrix} \\ &\times\begin{pmatrix}j_1&1&j_1'\\-m_{j_1}&m_{j_1}-m_{j_1}'&m_{j_1}'\end{pmatrix}\begin{pmatrix}j_2&1&j_2'\\-\omega_{j_2}&0&\omega_{j_2}\end{pmatrix}\begin{pmatrix}j_2&1&j_2'\\-m_{j_2}&m_{j_2}-m_{j_2}'&m_{j_2}'\end{pmatrix}.\end{aligned} \tag{13}$$

The multichannel interaction is illustrated in Fig. 3 by showing the lowest adiabatic energies of the symmetrized combined molecular state $|8,8,\eta=+1\rangle$ as a function of r at a magnetic field of $B=500$ G, for the electric fields $E=0,2,3$ kV/cm and different orientations $\theta_{EB}=0,\pi/4,\pi/2$. These curves are obtained by diagonalizing the matrix $\mathcal{U}(r)$ for each r. The thin solid black line shows the result for zero electric field $E=0$ kV/cm illustrating its repulsive C_6/r^6 behavior [8]. When the electric field is turned on, second-order perturbations induce an attractive C_4/r^4 [13,28] coming from a mixing of the $l=0$ and 2 partial waves of the dipole-dipole interaction. This interaction becomes increasingly attractive as the electric field grows and also when the magnetic field is more parallel to the electric field. This fact follows qualitatively from the induced electric dipoles of these state, as discussed for Fig. 2: For perpendicular fields, the electric dipole moment is harder to induce, hence the weaker attractive C_4/r^4 interaction, while for parallel fields the reverse is true.

The set of coupled equations (11) is solved for each r using a diabatic method, using the standard method of the propagation of the log-derivative matrix [29]. Matching the log-derivative matrix with asymptotic solutions at large r yields finally the scattering matrix S and the elastic and total

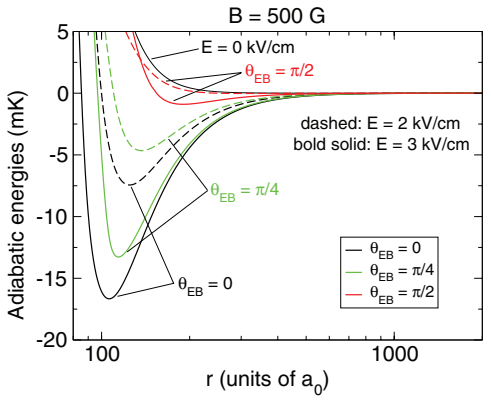

FIG. 3. (Color online) Adiabatic energies correlating to the $|8\rangle + |8\rangle$ combined molecular state as a function of the intermolecular separation r for $\theta_{EB} = 0$ (black curve), $\theta_{EB} = \pi/4$ [green (light gray) curve], and $\theta_{EB} = \pi/2$ [red (dark gray) curve] and different electric fields (thin solid: $E = 0$ kV/cm, thin solid curve; $E = 2$kV/cm, dashed curve; and $E = 3$ kV/cm, thick solid curve). The magnetic field is $B = 500$ G.

inelastic cross sections and rate coefficients, which are shown in the next section. Note that *ab initio* calculations are not precise enough at such cold temperatures ($T \leqslant 1$ K) to rule out the presence of a potential energy barrier in the entrance channel that could prevent the chemical reaction OH + OH $\rightarrow$ O + H_2O from occurring [30]. While we do not consider the possibility of chemical reactions in the present study, they could be considered in future works by using, for example, an absorbing condition at short range [28].

III. APPLICATION TO COLD AND ULTRACOLD OH + OH MOLECULAR SCATTERING

To better orient the discussion of scattering, consider the scales of electric and magnetic fields as seen by the OH molecule. For a prototypical cold collision energy $E = 1$ mK, this energy is the same as the Stark energy $|\vec{d} \cdot \vec{E}|$ for a dipole moment $|\vec{d}| = 1.67$ D and an electric field $E = 0.0247$ kV/cm and it is the same as the Zeeman energy $|\vec{\mu} \cdot \vec{B}|$ for a dipole moment $|\vec{\mu}| = 2\mu_B$ in a magnetic field $B = 7.4$ G. As a rule of thumb, one might therefore expect the magnetic field to have a dominant effect when $B/E \gg 300$ G/(kV/cm) and the electric field to have a dominant effect when the reverse is true.

The prospect of manipulating collisions via both electric and magnetic fields, possibly pointing in different directions, to say nothing of different collision energies, opens a large parameter space to consider. In this section we will explore different slices through this parameter space by varying separately the electric field magnitude, the magnetic field magnitude, and the relative orientation of the fields.

A. Scattering versus electric field

The general effect of increasing the electric field on scattering of OH is to increase the inelastic scattering rate. This effect arises because electric dipoles are induced, which exert the long-range torques on one another that drive state-changing collisions [13]. This effect is seen in Fig. 4, which shows the electric field dependence of the elastic and inelastic rate

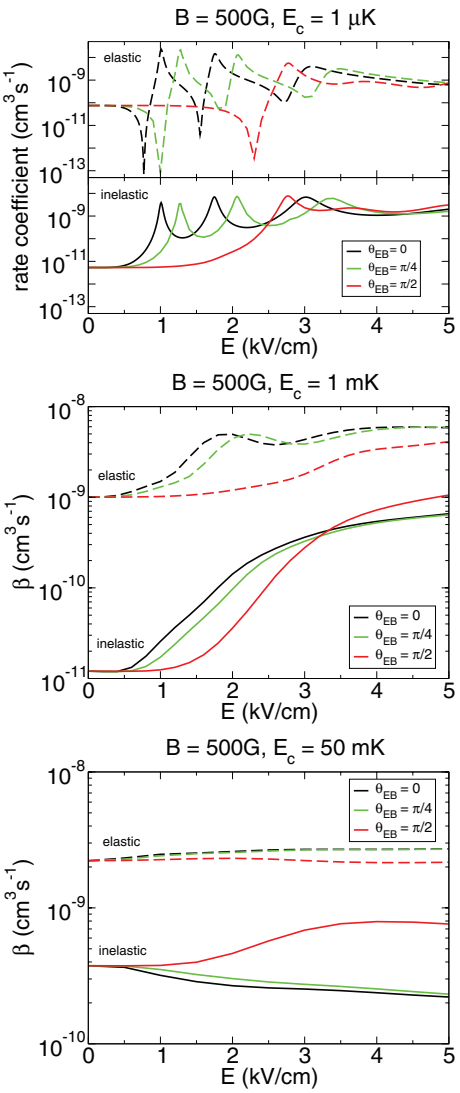

FIG. 4. (Color online) Rate coefficients as a function of electric field for $\theta_{EB} = 0$ (black curve), $\theta_{EB} = \pi/4$ [green (light gray) curve], and $\theta_{EB} = \pi/2$ [red (dark gray) curve]. The collision energy is $E_c = 1\mu$ K (top panel), $E_c = 1$ mK (middle panel), and $E_c = 50$ mK (bottom panel). The magnetic field is fixed to $B = 500$ G. Elastic process are plotted as dashed lines and inelastic processes are plotted as solid lines.

coefficients for $\theta_{EB} = 0$ (black curves), $\theta_{EB} = \pi/4$ [green (light gray) curves], and $\theta_{EB} = \pi/2$ [red (dark gray) curves] at different magnitude of collision energy for a fixed magnetic field $B = 500$ G. The three panels denote three different collision energies. At an ultralow collision energy of $E_c = 1\mu$ K, the rate coefficients show the presence of resonances, signaling the occurrence of long-range "field-linked" resonance states predicted in Ref. [13]. They correspond to the coincidence of virtual states with the collision energy as the electric field is turned on and as the adiabatic energy curves become more attractive (shown in Fig. 3).

The electric field values at which these resonances appear clearly depend on the angle θ_{EB} between the fields. As noted above, for more parallel fields it is easier to induce the electric dipole moments of the molecules and to obtain strong attractive

interaction curves, hence resonances appear at lower electric fields. Conversely, for more perpendicular fields the same resonances appear at higher electric fields since it is harder to induce the electric dipole moments and to obtain attractive interaction curves. Because of these resonances, the inelastic processes can be decreased by three orders of magnitude (see, for instance, at $E = 1$ kV/cm) between the parallel and perpendicular cases. The overall trend is a rise of the rates with the electric fields due to the increased dipolar coupling with other inelastic states as the electric field is turned on.

At a somewhat higher collision energy of $E_c = 1$ mK, the resonances are smoothed out since the width of scattering resonances usually increases as the collision energy increases [31]. The rise of the rates with the electric field is still visible. According to our rule of thumb, the electric field should exceed $\sim$1.7 kV/cm to exert a stronger influence on the molecules than a 500-G magnetic field. Indeed, the middle and bottom panels of Fig. 4 show suppressed inelastic rates below this field and enhanced rates above it. Details of the fields still matter, however. At a still larger collision energy, 50 mK, inelastic rates continue to be suppressed at high electric field, when the fields are not perpendicular.

B. Scattering versus magnetic field

As opposed to electric fields, magnetic fields tend to decrease the rate of inelastic scattering. This decrease is tied to the general separation of molecular states in a field, which reduces the Franck-Condon factors between initial and final states [14]. This effect, including its modifications due to the electric field, is shown in Fig. 5. This figure presents the magnetic field dependence of the elastic and inelastic rate coefficients for $\theta_{EB} = 0$ (black curves), $\theta_{EB} = \pi/4$ [green (light gray) curves], and $\theta_{EB} = \pi/2$ [red (dark gray) curves] for a fixed collision energy of $E_c = 1$ mK. In this figure each panel shows the result at a different electric field. The $E = 0$ kV/cm case is represented by a thin black line and of course does not depend on θ_{EB}.

The elastic rates are independent of the magnetic field, while the inelastic rates decrease with the magnetic field, in agreement with previous results of Ref. [14]. Considering the overall trends, our rule of thumb would suggest that the magnetic field suppression would become important at magnetic fields of 300, 900, and 1500 G for the three panels, respectively, and this is approximately what is seen. For $E = 1$ kV/cm, the trends of the rates are comparable and do not differ so much from the zero-field case. The electric field generates the largest deviation from the field-free case when the fields are parallel.

Once the electric field is larger, the angle between fields plays a more significant role. For $E = 3$ kV/cm, the rates of the $\theta_{EB} = 0$ and $\pi/4$ cases have globally increased with the electric field and show a moderate magnetic field dependence, while the rates of $\theta_{EB} = \pi/2$ have increased but still show a magnetic field dependence similar to lower electric fields. This is because the electric field is not strong enough for the perpendicular case to polarize the electric dipole moment and inelastic rates are still suppressed. Finally, for $E = 5$ kV/cm, the $\theta_{EB} = 0$ and $\pi/4$ cases show a weak magnetic dependence, while $\theta_{EB} = \pi/2$ still shows a certain dependence. For this case, one can see that for strong magnetic fields, one needs strong electric fields to get a strong electric dipole-dipole interaction to increase the inelastic rates.

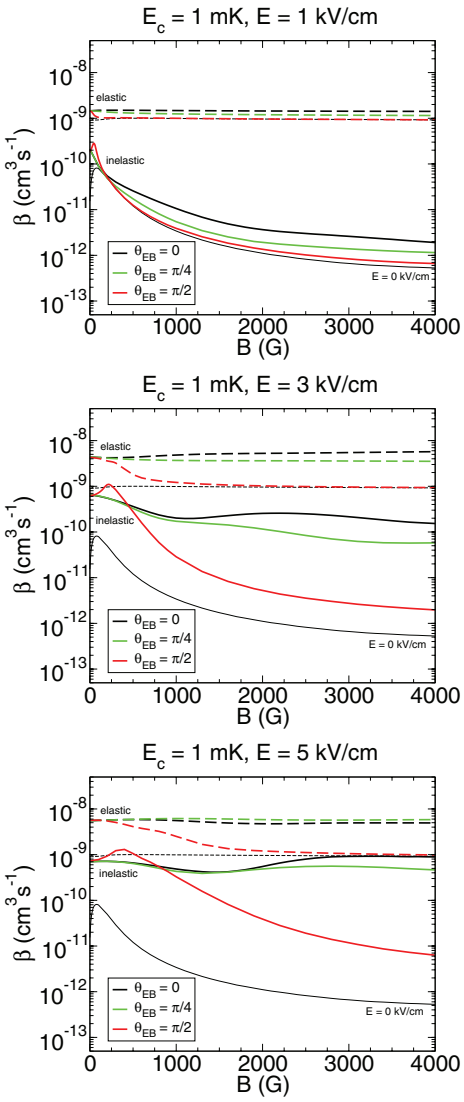

FIG. 5. (Color online) Rate coefficients as a function of magnetic field for $\theta_{EB} = 0$ (black curve), $\theta_{EB} = \pi/4$ [green (light gray) curve], and $\theta_{EB} = \pi/2$ [red (dark gray) curve]. The electric field is $E = 1$ kV/cm (top panel), $E = 3$ kV/cm (middle panel), and $E = 5$ kV/cm (bottom panel). The collision energy is fixed to $E_c = 1$ mK. The thin solid black line corresponds to $E = 0$ kV/cm. Elastic process are plotted as dashed lines and inelastic processes are plotted as solid lines.

C. Scattering versus the relative field orientations

Figure 6 presents the rate coefficient for different electric fields at a fixed magnetic field $B = 1500$ G and collision energy $E_c = 1$ mK, as a function of the fields angle θ_{EB}. For an electric field of $E = 1$ kV/cm, elastic and inelastic collisions depend weakly on the angle the electric field makes with respect to the magnetic field. The electric field is not strong enough to play a significant role since $B/E \gg 300$ G/(kV/cm), even though we see that the fields angle can have some effect on the inelastic rates, within a factor of 2–3.

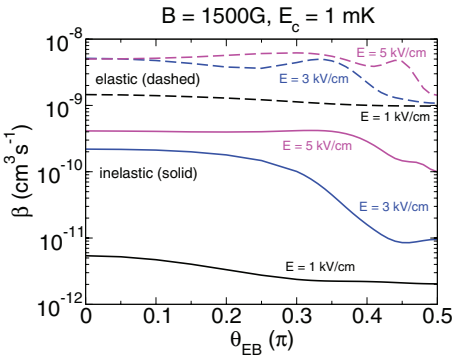

FIG. 6. (Color online) Rate coefficients as a function of the fields orientation for $E = 1$ kV/cm (black curve), $E = 3$ kV/cm [blue (dark gray) curve], and $E = 5$ kV/cm [pink (light gray) curve]. The magnetic field is $B = 1500$ G and the collision energy is $E_c = 1$ mK. Elastic process are plotted as dashed lines and inelastic processes are plotted as solid lines.

For an increased electric field of $E = 3$ kV/cm, the overall rates have increased from the low-electric-field case, but they decrease from $\theta_{EB} = 0$ to $\pi/2$, showing a strong anisotropy. Recall that in parallel fields, the magnetic field helps to polarize the molecules, thus increasing the inelastic rates. Molecular collisions strongly depend on the relative angle of the fields. For the same magnetic field, they can differ by one order of magnitude for the inelastic processes for example. Finally, at $E = 5$ kV/cm, where electric fields have an effect comparable to magnetic fields [$B/E = 300$ G/(kV/cm)], the inelastic rates are large and the angle dependence starts to weaken compared to the previous case of $E = 3$ kV/cm. In this case the electric field is strong enough to polarize the molecules along itself, so the strength and direction of the magnetic field start to become irrelevant.

D. Links with experiments

In experiments, polar molecules of OH are trapped in a magnetic quadrupole trap with spatially varying magnetic fields [8] and can be simultaneously subject to a uniform electric field [20]. At each location of the molecules in the trap, therefore, the molecules experience crossed fields of arbitrary magnitude and relative orientation, hence the different outcomes of two-body collisions as previously seen in this study. The fact that collision processes strongly depend on the position in the trap can be used to create nonuniform configurations of electric fields in magnetic traps so that high value of $\theta_{\rm EB}$ regions will favor elastic collisions, while low-value regions will favor inelastic ones. With proper field configurations, this could be used as a knife for evaporative cooling in such traps in order to remove the particles with the higher energy and keep the particles with the lower energy.

In such traps, it is somewhat more complicated to give an overall rate coefficient for a given temperature and for a given electric field since the molecular rate coefficients depend on the position of the trap as well as the collision energy. Experimental data of inelastic loss are now available for collision of OH molecules in a quadrupole trap and uniform electric fields [20]. To confront these data with theoretical predictions, one needs to consider the position- and velocity-dependent rate coefficients along with the proper phase-space distributions of molecular positions and velocities to describe molecular losses as a function of time. The option to consider or not the possibility of chemical reactions for OH + OH collisions will also play a role in the overall magnitude of the loss rates (inelastic plus reactive processes). This has to be kept in mind when comparing with experimental results.

In addition, one also needs to consider the time dynamics of the molecules inside the trap between collisions since elastic rates are higher than the inelastic ones and thus rethermalization plays an important role and since elastic scattering redistributes the velocity directions and magnitudes of the molecules according to the differential cross sections after a collision. Such calculations are more complex and usually require Monte Carlo simulations using classical trajectories [32,33]. This is beyond the scope of this paper.

IV. CONCLUSION

We have studied the collisions of electric and magnetic polar molecules in arbitrary configurations of electric and magnetic fields, taking the OH molecules as an example. The electric dipolar interaction depends on the way the electric dipole moments are induced. For the state considered in this study, it is easier to induce the electric dipoles when the electric and magnetic fields are parallel and this increases the strength of the molecule-molecule electric dipolar interaction. When the fields become perpendicular, it is harder to induce the electric dipoles along the electric field axis since the magnetic field tends also to align the molecular axis with it. This moderates the strength of the electric dipolar interaction. This is seen in the dynamics of OH + OH collisions where we found a strong dependence of the rate coefficients of elastic and inelastic processes on the electric and magnetic field configurations. For example, more parallel fields increase the inelastic processes, while more perpendicular fields moderate them. If the polar molecules are confined in a magnetic quadrupole trap in the presence of an electric field, the molecular collisions will be space and velocity dependent. Therefore, the molecular dynamics in such traps is complex. Elastic and inelastic collisions have to be taken into account as well as the motion of the particles between collisions in order to describe molecular loss and thermalization. This will be left for future investigations.

ACKNOWLEDGMENTS

This material is based upon work supported by the Air Force Office of Scientific Research under the Multidisciplinary University Research Initiative Grant No. FA9550-09-1-0588. This work was also supported in part by the National Science Foundation under Grant No. NSF PHY11-25915, during the "Fundamental Science and Applications of Ultra-cold Polar Molecules" program held at the Kavli Institute for Theroetical Physics, University of Santa Barbara, USA. G.Q. acknowledges Triangle de la Physique (Contract No. 2008-007T-QCCM) for financial support.

[1] G. Quéméner and P. S. Julienne, Chem. Rev. **112**, 4949 (2012).
[2] K.-K. Ni, S. Ospelkaus, M. H. G. de Miranda, A. Pe'er, B. Neyenhuis, J. J. Zirbel, S. Kotochigova, P. S. Julienne, D. S. Jin, and J. Ye, Science **322**, 231 (2008).
[3] S. Ospelkaus, K.-K. Ni, D. Wang, M. H. G. de Miranda, B. Neyenhuis, G. Quéméner, P. S. Julienne, J. L. Bohn, D. S. Jin, and J. Ye, Science **327**, 853 (2010).
[4] K.-K. Ni, S. Ospelkaus, D. Wang, G. Quéméner, B. Neyenhuis, M. H. G. de Miranda, J. L. Bohn, D. S. Jin, and J. Ye, Nature (London) **464**, 1324 (2010).
[5] M. H. G. de Miranda, A. Chotia, B. Neyenhuis, D. Wang, G. Quéméner, S. Ospelkaus, J. Bohn, J. L. Ye, and D. S. Jin, Nat. Phys. **7**, 502 (2011).
[6] A. Chotia, B. Neyenhuis, S. A. Moses, B. Yan, J. P. Covey, M. Foss-Feig, A. M. Rey, D. S. Jin, and J. Ye, Phys. Rev. Lett. **108**, 080405 (2012).
[7] E. S. Shuman, J. F. Barry, and D. DeMille, Nature (London) **467**, 820 (2010).
[8] B. K. Stuhl, M. T. Hummon, M. Yeo, G. Quéméner, J. L. Bohn, and J. Ye, Nature (London) **492**, 396 (2012).
[9] T. V. Tscherbul and R. V. Krems, J. Chem. Phys. **125**, 194311 (2006).
[10] E. Abrahamsson, T. V. Tscherbul, and R. V. Krems, J. Chem. Phys. **127**, 044302 (2007).
[11] T. V. Tscherbul, J. Chem. Phys. **128**, 244305 (2008).
[12] T. V. Tscherbul, J. Klos, L. Rajchel, and R. V. Krems, Phys. Rev. A **75**, 033416 (2007).
[13] A. V. Avdeenkov and J. L. Bohn, Phys. Rev. A **66**, 052718 (2002).
[14] C. Ticknor and J. L. Bohn, Phys. Rev. A **71**, 022709 (2005).
[15] T. V. Tscherbul, Y. V. Suleimanov, V. Aquilanti, and R. V. Krems, New J. Phys. **11**, 055021 (2009).
[16] J. Perez-Rios, J. Campos-Martinez, and M. I. Hernandez, J. Chem. Phys. **134**, 124310 (2011).
[17] L. M. C. Janssen, P. S. Zuchowski, A. van der Avoird, G. C. Groenenboom, and J. M. Hutson, Phys. Rev. A **83**, 022713 (2011).
[18] Y. V. Suleimanov, T. V. Tscherbul, and R. V. Krems, J. Chem. Phys. **137**, 024103 (2012).
[19] L. M. C. Janssen, A. van der Avoird, and G. C. Groenenboom, Phys. Rev. Lett. **110**, 063201 (2013).
[20] B. K. Stuhl, M. Yeo, M. T. Hummon, and J. Ye, Mol. Phys. (2013), doi:10.1080/00268976.2013.793838.
[21] A. V. Gorshkov, S. R. Manmana, G. Chen, J. Ye, E. Demler, M. D. Lukin, and A. M. Rey, Phys. Rev. Lett. **107**, 115301 (2011).
[22] M. A. Baranov, M. Dalmonte, G. Pupillo, and P. Zoller, Chem. Rev. **112**, 5012 (2012).
[23] M. L. Wall, E. Bekaroglu, and L. D. Carr, arXiv:1212.3042.
[24] J. M. Brown and A. Carrington, *Rotational Spectroscopy of Diatomic Molecules* (Cambridge University Press, Cambridge, 2003).
[25] J. L. Bohn and G. Quéméner, Mol. Phys. (2013), doi:10.1080/00268976.2013.783721.
[26] M. Lara, B. L. Lev, and J. L. Bohn, Phys. Rev. A **78**, 033433 (2008).
[27] A. V. Avdeenkov and J. L. Bohn, Phys. Rev. A **64**, 052703 (2001).
[28] G. Quéméner, J. L. Bohn, A. Petrov, and S. Kotochigova, Phys. Rev. A **84**, 062703 (2011).
[29] B. R. Johnson, J. Comput. Phys. **13**, 445 (1973).
[30] Y. Ge, K. Olsen, R. I. Kaiser, and J. D. Head, in *Astrochemistry: From Laboratory Studies to Astromomical Observations, Honolulu, 2005*, edited by R. I. Kaiser, P. Bernath, A. M. Mebel, Y. Osamura, and S. Petrie, AIP Conf. Proc. No. 855 (AIP, New York, 2006), p. 253.
[31] M. Mayle, G. Quéméner, B. P. Ruzic, and J. L. Bohn, Phys. Rev. A **87**, 012709 (2013).
[32] P. Barletta, J. Tennyson, and P. F. Barker, New J. Phys. **12**, 113002 (2010).
[33] H. Wu, E. Arimondo, and C. J. Foot, Phys. Rev. A **56**, 560 (1997).